

Evaluating the Robustness of LiDAR-based 3D Obstacles Detection and Its Impacts on Autonomous Driving Systems

Tri Minh Triet Pham, Bo Yang, Jinqiu Yang

Abstract—Autonomous driving systems (ADSs) require real-time input from multiple sensors to make time-sensitive decisions using deep neural networks. This makes the correctness of these decisions crucial to ADSs’ adoption as errors can cause significant loss. Sensors such as LiDAR are sensitive to environmental changes and built-in inaccuracies and may fluctuate between frames. While there has been extensive work to test ADSs, it remains unclear whether current ADSs are robust against very subtle changes in LiDAR point cloud data. In this work, we study the impact of the built-in inaccuracies in LiDAR sensors on LiDAR-3D obstacle detection models to provide insight into how they can impact obstacle detection (i.e., robustness) and by extension trajectory prediction (i.e., how the robustness of obstacle detection would impact ADSs).

We propose a framework *SORBET*, that applies subtle perturbations to LiDAR data, evaluates the robustness of LiDAR-3D obstacle detection, and assesses the impacts on the trajectory prediction module and ADSs. We applied *SORBET* to evaluate the robustness of five classic LiDAR-3D obstacle detection models, including one from an industry-grade Level 4 ADS (Baidu’s Apollo). Furthermore, we studied how changes in the obstacle detection results would negatively impact trajectory prediction in a cascading fashion. Our evaluation highlights the importance of testing the robustness of LiDAR-3D obstacle detection models against subtle perturbations. We find that even very subtle changes in point cloud data (i.e., removing two points) may introduce a non-trivial decrease in the detection performance. Furthermore, such a negative impact will further propagate to other modules, and endanger the safety of ADSs.

Index Terms—Software testing, system testing

I. INTRODUCTION

Automated driving systems (ADSs) have gained significant traction in both research and industry [1]–[3]. The rapid adoption of ADSs results in them being extensively studied due to their significant commercial value and the cost of their errors [4], [5]. In ADS, obstacle detection is critical and is largely responsible for the vehicle’s safety. Obstacle detection involves a complex system of different modules which may involve multiple sensors, and its output is critical to the performance of subsequent modules. Obstacle detection consists of using sensors to scan the environment, then process and analyze using deep neural networks (DNNs) to detect the obstacles. These obstacles are crucial for subsequent tasks such as trajectory prediction and path planning for appropriate interaction. A key component of this pipeline is 3D obstacle

detection, which uses light detection and ranging (LiDAR) sensors to capture the world around the ego car, which is then processed by DNNs to detect obstacles for further processing.

LiDAR obstacle detection is crucial to the operation of ADS due to their ability to accurately measure distance, work under low light conditions, and 360° view around the ADS. However, the output of LiDAR sensors is not perfect and often contains subtle built-in inaccuracies [6]–[8]. For example, Ouster OS2 specifications state that it has a range accuracy of three centimeters and precision that changes based on the distance of the object. Similarly, the Velodyne HDL-64E user’s manual states that it has a distance accuracy of five centimeters. This can be caused by various reasons including the difference in position, angle of capture, etc. of both the sensor and the obstacle between the start and the end of each LiDAR sweep. In addition, due to the complexity of the deployed environment of ADS (e.g., weather conditions in the world), since LiDAR sensors utilize lasers in their scan, color (and the material that produced the color) can significantly change how much light the sensor receives. Such built-in inaccuracies and subtle environmental impacts cause the produced PointClouds from LiDAR to fluctuate. Such fluctuated LiDAR outputs pose challenges to the robustness of the underlying DNNs models in ADS’s perception component. These seemingly harmless changes can change the outcome of the detection process. Yet, to the best of our knowledge, the effect of them on the output of 3D obstacle detection in particular, and on the rest of ADS is not yet evaluated in detail.

While there has been significant contribution in the area of adversarial attack on 3D obstacle detection [9]–[11], and attempts to benchmark 3D obstacle detection against various corruptions [1], [12], deviations that are caused by changes in color and very small perturbations, especially those local to the obstacles which are caused even when the sensors are operating correctly is not yet studied. Hence, in this work,

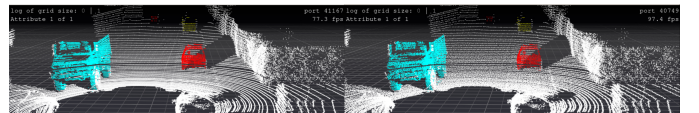


Fig. 1: **Left:** Original Velodyne point cloud from round 19 of KITTI data set. **Right:** perturbed point cloud using **global distance inaccuracy** where each point is moved less than two centimeters away from its original position.

we establish the first steps to bridge this gap by studying

TMT. Pham, B. Yang, and J. Yang are with the Department of Computer Science and Software Engineering, Concordia University, Montreal, Quebec, Canada. E-mail: p_triet, b_yang20, jinqiu@encs.concordia.ca.

the impact of these perturbations on the outcome of obstacle detection in a wide range of systems that are performing 3D obstacle detection. Also, leaning on these results, we are the first work to evaluate how such deviations that are the results of these errors can affect the performance of subsequent modules in ADS such as prediction and planning.

In this paper, we propose a framework (namely *SORBET*) to evaluate the robustness of LiDAR object detection modules against real-world fluctuations, and further assess the impacts on subsequent decision-making modules (i.e., planning and prediction) in ADS. We apply *SORBET* to evaluate the robustness of five representative LiDAR-based 3D obstacle detection models, including the model in an industry-grade ADS (Baidu's Apollo). Furthermore, we performed a simulation-based study to comprehensively assess the impact of deviated (even slightly) obstacle detection results on both models from academia such as Trajectron++ and an industry-grade ADS Apollo. We answer the research questions (RQs) below.

RQ1 (Robustness): How robust are LiDAR-3D obstacle detection models against subtle perturbations? In our experiment of four LiDAR-based 3D obstacle detection models and one industry-grade model in Apollo, we find that random perturbations less than two centimeters can cause up to 17.5% of change in the number of obstacles detected in well-known 3D obstacle detection models. When the perturbations are larger and more targeted, it can cause up to 23.5% change in the number of obstacles detected.

RQ2 (Impact on ADS): What are the cascading impacts on ADSs caused by the perturbations of the LiDAR's PCD input? Our study shows that while trajectory predictors are robust to most perturbations observed, very small built-in perturbations can still cause significant deviations in the trajectory prediction results.

RQ3 (Defense and retraining): Can the perturbations improve the robustness of ADSs? We find that retraining with the perturbations can improve the robustness of 3D obstacle detection models.

II. BACKGROUND AND RELATED WORK

In this section, we present the background of our study which focuses on two components in ADS, which are LiDAR 3D obstacle detection and trajectory prediction module. In addition to describing the necessary knowledge of these two modules, we detail prior works on testing and performing adversarial attacks on these two modules in ADS.

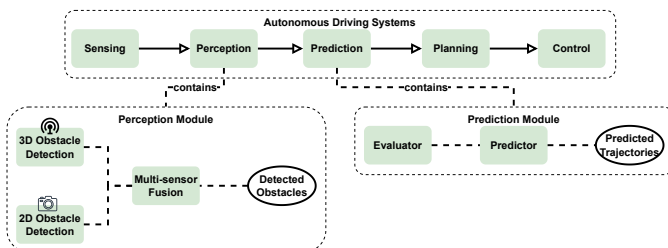


Fig. 2: An Overview of a typical ADS

A. LiDAR-3D obstacle detection

LiDAR-based 3D obstacle detection is crucial the the operation of ADS. At fixed intervals, the LiDAR sensors capture the environment via a “sweep,” which is a 360° scan of the environment. The data is stored as a point cloud (PCD), which is a large set of data points, each containing the 3D position (x, y, z dimensions) and the intensity, representing the reflected lights from various surfaces in the environment. The PCD is then processed by 3D obstacle detection systems to return 3D bounding boxes annotating the obstacles detected.

Testing LiDAR Obstacle Detection LiDAR obstacle detection has been subjected to significant testing efforts. These works benchmark obstacle detection models under corruptions and noises that can occur due to various reasons. Zhou and Sun [13] use metamorphic testing on LiDAR obstacle detection in Apollo by adding points in the PCD outside of the region of interest (ROI). Yu et al. [14] and Gao et al. [15] test the robustness of fusion obstacle detection systems using noisy/corrupted input data that comes from multiple sources (which includes noisy LiDAR input). Albreiki et al. [16] test general object detectors against various corruption patterns including addition, removal, and jitter. Sun et al. [12] test the LiDAR obstacle detection models under 15 different commonly occurring corruptions. In this work, we are testing the LiDAR obstacle detection process under the assumption that it is operating under normal conditions without interference. Our perturbations are not caused by external events but by the built-in inaccuracy of the instruments. From previous research, Sun et al. [12] would be closest to our work in that they introduce many types of corruption. However, while their works investigated multiple corruption types that are more visible (and would require interference/hardware failure to manifest) and measured the increase in the models’ error rate, our work focuses on mostly invisible, very small perturbations (that can happen when the instrument is operating under normal conditions) and how different patterns of such perturbations can influence different metrics from the output of 3D obstacle detection, even for those obstacles that are not considered detected via common metrics, and by extension, the remaining modules in ADSs.

Adversarial Attacks on LiDAR Obstacle Detection Significant efforts have been made to attack this module. Xu et al. [9] attack DNN-based segmentation obstacle detection models by adding points in the unnoticed areas. Cao et al. spoofed obstacles to the PCD [10] and both LiDAR and camera obstacle detection [11]. Zheng et al. [17] propose an adaptive gradient attack algorithm that can identify vulnerable regions in the PCD and generate local perturbations to attack those regions. Shin et al. [18] attack LiDAR by spoofing objects and creating illusions in LiDAR output. Sun et al. [19] utilize occlusion patterns from data sets to attack obstacle detection models. Wang et al. [20] introduce loss-function guided perturbations to obstacle PCDs to induce failure in the detection process. Zhu et al. [21], [22] identify physical locations in the PCD where occlusion or reflection can change the detection results and attack those locations. Yang et al. [23] perturb small roadside obstacles to make obstacle detection

models misidentify them as vehicles, causing unexpected reactions from ADS. Hau et al. [24] induce failure in obstacle detection by introducing points behind the obstacles, shifting the obstacles. Xiong et al. [25] propose a GAN-based attack on both the LiDAR and camera obstacle detection modules. Abdelfattah et al. [26] generate adversarial obstacles that can attack both LiDAR and camera detection. Tu et al. [27], [28] place objects with adversarial shapes on obstacles to disrupt the PCD. Liu et al. [29] generate camera perturbations and project them to the 3D space to attack 3D obstacle detection. Our work does not involve attacking the LiDAR obstacle detection process. We are testing their robustness under normal operating conditions.

B. Trajectory prediction

Trajectory prediction is a core component in ADSs. Depending on the organization, it can be part of another module or standalone as in the case of Apollo. The main task of these types of systems is to predict the position of the detected obstacles in the next few seconds based on their position in the last few seconds. Optional features that may be leveraged include heading, velocity, map information, ego position, etc. In Apollo, the prediction module [30], [31] predicts trajectories of all the obstacles detected by the perception module using perception information including positions, headings, velocities, etc. The prediction module comprises four main functionalities: container, scenario, evaluator, and predictor. Container stores input data from subscribed channels including perception obstacles. The scenario sub-module analyzes scenarios that include the ego vehicle and classifies it based on the possibility of the obstacle affecting the ego's planning trajectory (relative distance and whether the obstacle is on the same lane as the ego) and whether the ego car is at a junction. The evaluator predicts the path and speed for detected obstacles using the given model. In Apollo, ten evaluator models are used depending on the type of obstacle and the situation presented by the scenario sub-module. The predictor generates predicted trajectories for obstacles.

Adversarial Attacks on Trajectory Prediction. After the obstacles are detected, ADSs would determine whether these obstacles will interact with the planned path via trajectory prediction. There have been several works that attack this module since the output of this will affect the reaction of the ego car. Zhang et al. [32] propose an adversarial attack that perturbs vehicle trajectories to maximize error in trajectory prediction. Their evaluation of three models and three data sets shows that the method increases the prediction error by more than 150% and can generate unsafe driving decisions. Jia et al. [33] generate patches to attack obstacle tracking that can cause collisions and unnecessary stops. Then, some works attack trajectory prediction by modifying the PCD input. Li et al. [34] spoof ego car's trajectory with small perturbations to make it fail to detect safety-critical obstacles correctly. Wang et al. [35] generate adversarial perturbations to the trajectory and project those changes to the LiDAR input for a full system attack. Saadatnejad et al [36] attack social-aware pedestrian trajectory prediction systems. We are not proposing an attack on the trajectory prediction module.

Testing Trajectory Prediction While significant effort is invested in attacking trajectory prediction systems, few test the module. Han and Zhou [37] leverage metamorphic testing to detect unavoidable collisions due to bugs in Apollo's planning and prediction modules by adding and removing static obstacles within stopping range and see if the ADS can react. Jiao et al. [38] propose a semi-supervised, auto-encoder-based adversarial training method for the trajectory prediction modules, which enhances their robustness and mitigates the impacts of attacks on the trajectory. In this paper, we seek to test the robustness of trajectory prediction by introducing perturbations that come from our measurements of the deviations caused by built-in instrumental inaccuracies, and our experiments seek to quantify the impact of such perturbation on the trajectory.

III. SORBET: A FRAMEWORK TO EVALUATE THE ROBUSTNESS OF LiDAR 3D OBJECT DETECTION

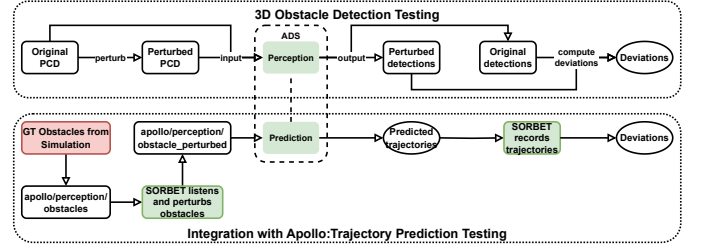


Fig. 3: Overview of SORBET framework.

In this section, we present the design of *SORBET* as (1) a standalone framework for evaluating the robustness of LiDAR-3D obstacle detection and further assessing its impacts on trajectory prediction; and (2) a complete integration with Apollo (an industry-grade multi-module ADS) in a simulator environment. Figure 3 illustrates the major components of *SORBET*: perturbation injection to PCD (model input), Executing obstacle detection model, Comparing the detection results (with and without perturbations), and calculating the evaluation metrics.

A. Types of perturbations to be injected into the PCD

From LiDAR manuals and prior studies that investigate the inaccuracies of LiDAR sensors, we conclude four types of *subtle* and *common* perturbations that can cause the PCD from LiDAR to slightly fluctuate over time (i.e., frame to frame). Even the slightest fluctuations in the PCD may cause obstacle detection models to be dysfunctional, as illustrated by prior work on generating adversarial attacks [10]. *Such slight fluctuations (LiDAR built-in inaccuracies, environment noise, reflectivity noise) are realistic to naturally expand the test space of collected PCDs and complement prior techniques [15], [39] that evaluate the robustness of LiDAR 3D obstacle detection against extreme weather (e.g., fog, raining) or external equipment attacks (e.g., lasers).*

We generate the perturbations as follows. First, we obtain the raw PCD from the 3D object detection benchmark KITTI data set [7]. Second, we read the Velodyne PCD as matrices

of coordinates. For each perturbation type in Table I, we generate several perturbation matrices with the same shape as the original PCD. We then apply the perturbation depending on the type and scope of the perturbation and save it as the perturbed PCD. We use these generated perturbed PCD as the models' input and evaluate the resulting deviations. Next, we describe the designed perturbations in detail.

TABLE I: The perturbations included by *SORBET*. We design perturbations to reflect subtle environment noise and LiDAR inaccuracies from prior studies and manuals [6]–[8].

Perturbation	Scope	Distribution	Description
range inaccuracy	global, local, direction	uniform, Gaussian, Laplacian	Add perturbations to select points in PCD
false positive	global, local	uniform	Remove select points from PCD
reflectivity noise	direction of absorption	uniform	Add or remove a percentage of points from obstacles' PCD to simulate different obstacle colors
distance-amplified range inaccuracy	local	uniform	Add perturbations local to obstacles' PCD based on distance from sensor

Range inaccuracy (global, local, and directional). LiDAR sensors produce very subtle inaccuracies [6]–[8]. There are many factors contributing to the range inaccuracy: imperfect calibration, angles, and viewpoints of LiDAR hardware, as well as latencies and processing errors of LiDAR software. We design the perturbation to replicate range inaccuracy by shifting the (x, y, z) coordinates of a set of selected points from PCD. The shift is bounded by pre-defined ranges, i.e., $[-0.02, 0.02]$ meters, which is concluded by the specifications of popular LiDAR sensors [6] such that the combined shift from the three dimensions does not exceed this range. This set of points is selected following one of the three distributions (uniform, Gaussian, and Laplacian), which are commonly used to simulate environment noises [40]–[42]. We use three types of scopes for these perturbations. (1) **Global**. We apply the distributions to the entire PCD (i.e., between 100,000 and 120,000 points) for selecting a set of points and then shift the x and y coordinates of these selected points. (2) **Local**. Unlike global, we only apply the distributions to a much-restricted region, i.e., the annotated obstacles in PCD. This may be most similar to previous work, i.e., corruptions in [12]. However, our designed perturbations have different applied regions and smaller distances, i.e., the max shift of xyz combined is 0.02 m for our method, compared to 0.05 m to a single dimension x in [12] under the lowest noise configuration. We applied a z-test to compare our perturbed PCDs and [12]. For example, applying z-test on the perturbations generated from 'Noise Corruption' [12] and this perturbation achieves an average z-score of -62 with a p-value of 0, which shows a difference with statistical significance. (3) **Directional**. We still apply the shift only to the selected points in the obstacles. Differently, the perturbations within the same obstacle will have the same direction, e.g., moving all the selected points to positive x by 2cm. This directional perturbation is to replicate range inaccuracies caused by LiDAR hardware issues (e.g., calibration and view angles). In our experiment, we apply these perturbations in six directions, i.e., $\pm x$, $\pm y$, and $\pm z$.

False positives (global and local). This perturbation means that for every point that we get in the PCD, there is a chance that it is a false positive, thus showing a point that is not supposed to be there. To represent this phenomenon, we randomly remove one point out of 10,000 points as shown in the manual [6].

Reflectivity noise (direction of absorption). Since LiDAR uses laser scans to sense the environment, it inherently suffers from reflectivity noises due to the materials and color of the obstacles and lighting conditions. Such environmental variables cause the surface of the obstacles to have a slightly different absorption rate from frame to frame. As a result, it affects the reflectivity and changes the intensity of the return laser. This can change whether the receiver on the sensor can capture it. From our investigation, we learn from previous work [43] that the number of points representing an obstacle is different depending on its color. We are unable to find the actual number/percentage of points representing an obstacle of each color and material and by extension the actual percentage of the change in the number of points in the PCD. Hence, in this work, we apply the following perturbations based on the following assumptions with numbers as described in Sequeira et al. [43].

Decreased reflectivity: We assume that the material, color, lighting, etc. of the obstacles is changed so that the reflectivity is decreased, reducing 60% of the points in corresponding obstacles, e., the color changes from white to black.

Increase reflectivity: We assume that the reflectivity is enhanced, increasing the number of points in those obstacles by 67%.

Distance-amplified range inaccuracy. Common photonic effects such as the diffusion of light on complex surfaces significantly impact how light is being reflected to a LiDAR sensor. This causes diverse range inaccuracies based on the distance and angle between an obstacle and the ego car. This perturbation is more sophisticated than the regular range inaccuracy since it is only applied to a subset of the obstacles in the PCD. While we have not been able to locate experiments or documentation that quantify the amount, we leverage the difference in the precision observed in the OS2 LiDAR sensor to simulate this imperfection [6]. For this perturbation, depending on the distance between an obstacle and the ego car, we apply a corresponding distance-amplified value to shift the PCD points.

B. Identifying the regions of PCD that represent obstacles

Some perturbation types in *SORBET* are only applied to the PCDs representing the obstacles as described in the ground truth. To do this, we locate the points representing the obstacles from the PCD by obtaining the 3D bounding box representing the obstacles in the LiDAR coordinates via the following steps. From the ground truth bounding box in camera coordinates from KITTI, we compute 3D projections of the obstacles using the provided calibration files and instructions. Then, from the 3D bounding boxes representing the obstacles, we can extract the point cloud representing the obstacles in the original PCD. Thus, we can add perturbations

local to the obstacles by applying the generated perturbations only to these points.

C. Calculating the detection differences caused by perturbations

In standard procedures, an obstacle is detected if compared to the ground truth, its intersection-over-union (IoU) (a common metric to determine obstacle detection) is greater or equal to 0.7 for cars and 0.5 for cyclists and pedestrians. This applies to obstacles detected both before and after perturbations. However, in this paper, we are not interested only in when the obstacle is detected/undetected, but we want to keep track of changes and deviations even when the detection status of the obstacle changes or it has never even been detected as shown in Table III. In the table, we can see that even using unaltered KITTI data, each model has a different number of detected obstacles. Hence, in this table, except when we compute detected obstacles (*Det. Obs*) or the difference in the number of detected obstacles before and after perturbation (*Det. Diff*), we would compute the deviation metric using obstacles with the same ground truth ID as long as the IoU is greater or equal to 0.25. This means that $x, y, z, size, IoU$ in Table I are computed using this threshold. We use the threshold of 0.25 as a compromise since otherwise at 0, the matched obstacles are not likely to be the same obstacle.

D. Applying SORBET on an industry-grade ADS

We envision *SORBET* as a framework to not only evaluate the robustness of obstacle detection but also expand to evaluate the impacts of obstacle detection results on other parts of ADS. Hence it is important to apply *SORBET* on a complete ADS in addition to individual DNN models for obstacle detection and trajectory prediction. We chose to evaluate Baidu's Apollo and use the LGSVL simulator for running Apollo in simulated environments, both commonly used in prior works [1]. LGSVL by far still works best with Apollo. However, it is not limited to LGSVL and can be extended to work with CARLA [40]. In short, *SORBET* does not tie with one particular simulator, but rather which simulator would work with Apollo.

Testing Apollo's obstacle detection module. We leverage existing testing code in Apollo to load the point cloud and run 3D obstacle detection. Using the same process as described in Figure 3, we provide Apollo's CNN segmentation model with the original and perturbed PCDs and calculate the 3D bounding box and IoU with the ground truth from the results. From this, we can compute the resulting deviations from the same perturbations as applied in other models.

Testing Apollo's trajectory prediction module. To integrate with Apollo, we deactivate the perception, camera, and traffic light modules in Apollo. Then, we leverage the LGSVL simulator to provide the ground truth information to Apollo as the output of the mentioned modules. Doing this ensures 100% the correctness of the obstacle detection process from the *apollo/perception/obstacles* channel in Apollo.

We introduce the perturbation we found to the input of Apollo's prediction module as follows. First, we create a listener using Apollo's CyberRT [30] which listens to *apollo/*

perception/obstacles (1). Second, we redirect the input channel of the prediction module from (1) to *apollo/perception/obstacles/obstacle_changed* (2). When we do not want to introduce perturbations, we redirect the data from (1) to (2) directly. However, when we want to introduce perturbations to the obstacles, we can modify it when we receive it from (1) before redirecting it to (2). The flow is also summarized in Figure 3. Similar to the process of recording the trajectories for obstacles, we set up a new listener for the channel *apollo/prediction* and record the predicted trajectory of each obstacle the prediction module received as input.

IV. EXPERIMENT SETUP

Computing Environment. We experiment on an Ubuntu 20.04.3 LTS system with an AMD Ryzen 16-core CPU, 256 GiB of memory, and an NVIDIA GeForce RTX 3090.

Data Sets. We use three different data sources for various tasks as shown in Table II. KITTI 3D Object Detection Evaluation 2017 (KITTI) [7] is an obstacle detection benchmark widely used in literature [1]. This contains 7,481 frames where 3,712 frames are for training and 3,769 frames are for testing & evaluation. Testing trajectory prediction requires a series of consecutive frames. Since KITTI provides single-frame PCD only and thus is unsuitable to test the trajectory prediction, we utilize nuScenes Prediction Challenges (nuScenes) [8]. nuScenes is a well-known benchmark of 150 scenes, each containing multiple frames showing the path of obstacles.

TABLE II: Data sets used. Vehs: vehicles. Peds: pedestrians

Target Module	Data set	Year	Instances	Obs. Count
Obstacle detection	KITTI [7]	2012	3,769 frames	Vehs: 16,895
				Peds: 2,446 Cyclists: 893 Misc.: 636
Trajectory prediction	nuScenes [8]	2020	150 scenes	Vehs: 2,016
	LGSVL [44]	2021	1 scene	Peds: 1,814 Vehicles: 1

TABLE III: Details of our evaluated models for obstacle detection and trajectory prediction. The performance is the R11 3D mAP (car/pedestrian/cyclist) for moderate cases evaluated on the KITTI data set.

Model Type	Model Name	Year or Version	Performance
Obstacle detection	Point Pillar [45]	2019	77.28/52.29/62.68
	Point RCNN [46]	2019	78.70/54.41/72.11
	Voxel RCNN [47]	2020	84.54 (cars only)
	TED [48]	2023	87.99 (cars only)
	Apollo's CNN Segmentation [30]	V5.5	unknown
Trajectory prediction	Trajectron++ [49]	2020	NA
	Apollo's Trajectory Prediction [30]	since V3.5	NA

Evaluated Subjects. We experiment on five pre-trained LiDAR-3D obstacle detection models with diverse DNN architectures (Table III). We obtained the four academia models through OpenPCDet [50] which is an open source, PyTorch-based code base for 3D object detection from point cloud.

We select the following models. PointPillar, a 3D obstacle detection model previously used in Apollo V6 [30]. In addition, we pick PointRCNN [46] and VoxelRCNN [47] from the OpenPCDet model zoo. Also, we select TED [48] which is highly ranked on the the KITTI 3D obstacle detection leaderboard. For industry-grade ADS, we pick Apollo Version 5.5 which uses a CNN segmentation model for LiDAR-3D obstacle detection. Apollo V5.5 has been popularly evaluated in prior works on ADS testing [1], [51].

For trajectory prediction, we select Trajectron++, a popular trajectory prediction model [32], [34], [49]. Also, we select Apollo's trajectory prediction which is a part of a production-grade L4 system and has been used since Apollo 3.5.

At the end of our selection process, we arrived at a set of 3D obstacle detection systems that are well-known and represent different types of techniques in 3D obstacle detection.

Evaluating the LiDAR-3D obstacle detection models on KITTI. We run the pre-trained models from the model zoo. We only add noises to the PCD as described in Section III-A. To accurately measure our result, for the baseline and each perturbation described, we run each model on the KITTI data set five times to account for instability in model detection where the detection results from identical input does not result in the same detection results. This phenomenon may occur depending on the model. For example, for PointPillar, the results obtained from all five runs using identical input are identical; on the other hand, for PointRCNN, we observe the difference in the number of obstacles detected to be between four and seven obstacles.

We run each model on the baseline and each perturbed version of the KITTI data set to obtain the obstacles detected by the model (irrespective of their IoU), their position, intersection-over-union (IoU), and various other metrics. On average, we observe the average run time for each frame is between 0.02-0.03 seconds for PointPillar, PointRCNN, and Voxel-RCNN, 0.09 seconds for TED, and 0.46 seconds in the case of Apollo due to larger overhead in our set up. The presented data is the median of the recorded results.

Establishing the baseline for deviation comparison For further evaluation of the impact of the perturbations, we establish a baseline for each model in Table III. We run each model on the unaltered KITTI data set and record the results as described. These metrics are used for comparison when perturbations are added to the input. The deviation is the result of perturbations compared to this baseline. The baseline for the number of obstacles detected is shown in Table III.

V. EVALUATION RESULTS

RQ1: How robust are LiDAR-3D obstacle detection models against subtle perturbations?

Motivation. Even small perturbations between one and two centimeters may change the detection results of obstacle detection models. From documentation of popular LiDAR sensors such as Velodyne HDL-64E or OUSTER OS2 [6], we learn that the sensors, while highly accurate, still have built-in noise. This inaccuracy can be up to ten centimeters. Furthermore, the KITTI data set [7] (which was recorded by the Velodyne HDL-64E) and the NuScenes data set [8] (which was recorded by

Velodyne HDL-32E) both state that their recordings distance accuracy of two centimeters.

From this, in the first step of the experiment, we will evaluate minute built-in perturbations of LiDAR sensors' impact on the detection results. Then, we will investigate an area that has not been thoroughly investigated where the perturbations only affect the PCD local to the obstacle while the rest of the PCD remains undisturbed. Those interferences are local to the obstacles, e.g., how the obstacles reflect light to the sensor. This can be caused by the shape, color, distance, etc. of the obstacle. These perturbations are more specific to obstacles, representing many natural events that can happen to the PCDs representing the obstacles such as slight shifts of the entire obstacles within two centimeters, obstacles having different colors, etc. as described in Section III-A.

Method. We applied *SORBET* to generate PCD from KITTI with subtle perturbations. In each iteration, only one perturbation is applied to produce one perturbed PCD. This is to minimize the perturbations and enable individual evaluation of each built-in inaccuracy. It remains future work to evaluate the impact of combinational perturbations on LiDAR model performance. There are a total of 3,769 unique frames in KITTI. *SORBET* generates a total of 3,769 x 15 frames of perturbed PCD.

The KITTI dataset has almost 20K obstacles and the evaluated models (Table II) detect between 9,777 and 13,296 obstacles. For each evaluated model, for each frame, *SORBET* compares all obstacles pair-wise. To evaluate the deviation from perturbations, we record the baseline for each system for each metric (x, y, z, size, IoU, etc.). Then, we compute the deviation (e.g., $|\hat{x} - x|$) obtained for each obstacle. *SORBET* calculates the following evaluation metrics.

- 1) For the x, y, and z dimensions, as well as the size and IoU, the deviation is calculated as the absolute difference, such as $|\hat{x} - x|$.
- 2) Large deviation count (LDC) is the count of obstacles with any dimensions (x, y, z) that deviate more than a defined threshold. We set the threshold as 0.1 m.
- 3) Detection differences (DIFF) is the count difference (via ground-truth matching) between the obstacles detected by models from PCD w/o and w/ perturbations.

Results. Table IV shows the robustness results of our study using *SORBET*. Note that for x, y, z, size, and IoU, we present the median. LDC and DIFF are aggregated metrics based on the detection results. Our evaluation shows that across the models, **we observe up to 23.5% fewer obstacles detected**. Failing to detect obstacles is likely to introduce adverse consequences on ADS. TED [48] (the newest) is the most robust (lowest DIFF obstacles) among evaluated models against the current perturbations by *SORBET*. Apollo's CNN segmentation model result is worse than TED's but has comparable robustness compared with Voxel RCNN [47].

For the deviations on x, y, and z dimensions, we focus on the large deviations (more than 0.1 m), and the median value is presented in Table IV. The rationale is that for all the perturbations we designed in *SORBET*, the maximum shift introduced is 2cm. Thus, we focus our analysis on cases with deviations at least five times the maximum perturbation value

TABLE IV: Summary of the large deviations caused by random perturbation on obstacle detection. ‘FP’ is short for false positive. ‘Refl.’ is short for reflectivity noise. ‘Dist.’ is short for distance-amplified range inaccuracy.

		Range Inaccuracy									FP Local	Refl. (↓) (↑)		Dist. Unif.
		Unif.	Global Norm.	Lapl.	Unif.	Local Norm.	Lapl.	Unif.	Directional Norm.	Lapl.				
PointPillar	x	0.16	0.16	0.16	0	0.16	0.15	0.15	0.15	0.15	0	0.16	0.15	0.16
	y	0.13	0.14	0.14	0	0.14	0.15	0.14	0.15	0.15	0	0.16	0.16	0.14
	z	0.12	0.12	0.12	0	0.11	0.18	0.13	0.12	0.12	0	0.12	0.15	0.12
	size	0.39	0.40	0.38	0	0.38	0.40	0.40	0.41	0.40	0	0.65	0.61	0.41
	IoU	0.06	0.06	0.05	0	0.05	0.06	0.05	0.05	0.05	0	0.06	0.05	0.06
	LDC	409	799	768	0	409	388	489	940	913	0	5,661	735	1,204
		2.3%	4.5	4.4%	0%	2.3%	2.2%	2.8%	5.3%	5.2%	0%	32.1%	4.2%	6.8%
	DIFF	1,278	816	794	0	391	421	453	279	261	0	2,768	537	842
		9.6%	6.1%	6.0%	0%	2.9%	3.2%	3.4%	2.1%	2.0%	0%	20.8%	4.0%	6.3%
Point RCNN ¹	x	0.15	0.14	0.15	0.13	0.14	0.14	0.14	0.14	0.13	0.11	0.16	0.14	0.15
	y	0.14	0.13	0.14	0.13	0.13	0.13	0.13	0.12	0.12	0.13	0.15	0.14	0.14
	z	0.13	0.13	0.13	0.15	0.12	0.13	0.13	0.11	0.12	0	0.13	0.13	0.13
	size	0.64	0.65	0.64	0.44	0.62	0.58	0.61	0.62	0.63	0.46	0.83	0.64	0.63
	IoU	0.05	0.06	0.06	0.04	0.05	0.05	0.05	0.05	0.06	0.03	0.06	0.05	0.06
	LDC	2,297	3,105	3,109	17	2,401	2,398	2,771	3,428	3,316	19	4,556	3,281	3,623
		14.1%	19.1%	19.1%	0.1%	14.8%	14.8%	17.1%	21.1%	20.4%	0.1%	28.1%	20.2%	22.3%
	DIFF	2,285	1,819	1,786	20	1,408	1,292	1,521	1,267	1,204	17	3,072	1,717	1,786
		17.5%	13.9%	13.7%	0.2%	10.8%	9.9%	11.7%	9.7%	9.2%	0.1%	23.5%	13.2%	13.7%
Voxel RCNN	x	0.14	0.14	0.14	0	0.15	0.14	0.15	0.15	0.15	0	0.16	0.14	0.14
	y	0.14	0.14	0.13	0	0.13	0.13	0.13	0.14	0.13	0	0.16	0.14	0.13
	z	0.11	0.12	0.11	0	0.11	0.13	0.12	0.11	0.12	0	0.13	0.13	0.12
	size	0.48	0.56	0.55	0	0.49	0.50	0.48	0.55	0.54	0	0.77	0.65	0.55
	IoU	0.06	0.06	0.06	0	0.05	0.06	0.05	0.05	0.06	0	0.06	0.05	0.06
	LDC	691	1,082	981	0	658	613	570	923	891	0	3,910	984	2,025
		4.7%	7.4%	6.7%	0%	4.5%	4.2%	3.9%	6.3%	6.1%	0%	26.8%	6.7%	13.9%
	DIFF	587	762	747	0	533	529	504	701	688	0	1,786	617	1,025
		4.9%	6.4%	6.3%	0.0%	4.5%	4.4%	4.2%	5.9%	5.8%	0.0%	15.0%	5.2%	8.6%
TED	x	0	0.13	0.13	0	0.14	0.15	0.12	0.12	0.13	0	0.15	0.14	0.14
	y	0	0.13	0.14	0	0.14	0.15	0.13	0.15	0.15	0	0.14	0.12	0.13
	z	0	0.13	0.13	0	0.18	0.12	0.12	0.19	0.14	0	0.15	0.13	0.13
	size	0	1.03	1.13	0	0.47	0.60	0.44	0.50	0.55	0	0.83	0.63	0.52
	IoU	0	0.05	0.05	0	0.06	0.07	0.06	0.06	0.06	0	0.06	0.05	0.06
	LDC	0	237	246	0	94	95	86	99	101	0	1,540	104	505
		0%	1.6%	1.7%	0%	0.6%	0.6%	0.6%	0.7%	0.7%	0%	10.4%	0.7%	3.4%
	DIFF	0	394	407	0	255	246	240	260	259	0	1,275	236	508
		0.0%	3.0%	3.1%	0.0%	2.0%	1.9%	1.8%	2.0%	2.0%	0.0%	9.8%	1.8%	3.9%
Apollo ¹	x	0.19	0.21	0.20	0.20	0.22	0.21	0.20	0.21	0.22	0.19	0.22	0.21	0.19
	y	0.17	0.17	0.18	0.17	0.17	0.16	0.16	0.16	0.17	0.15	0.16	0.17	0.18
	z	0.17	0.16	0.16	0.16	0.16	0.16	0.16	0.17	0.16	0.16	0.16	0.17	0.16
	size	0.80	0.80	0.80	0.77	0.78	0.76	0.75	0.76	0.75	0.72	0.96	0.77	0.81
	IoU	0.03	0.02	0.02	0.02	0.02	0.02	0.02	0.02	0.02	0	0.13	0.02	0.04
	LDC	1,886	1,924	1,864	1,570	1,590	1,567	1,615	1,621	1,596	1,510	3,431	1,716	1,683
		15.6%	16.0%	15.5%	13.0%	13.2%	13.0%	13.4%	13.4%	13.2%	12.5%	28.4%	14.2%	14.0%
	DIFF	638	623	667	379	387	372	400	403	398	245	1,967	402	641
		6.5%	6.4%	6.8%	3.9%	4.0%	3.8%	4.1%	4.1%	4.1%	2.5%	20.1%	4.1%	6.6%

¹ Measurements represent the median of five rounds using identical input.

(ten centimeters). Deviations between two and ten centimeters are not as impactful as we are interested in learning how large deviations can be given very small perturbations to the input. **Our results show that the amplification effect, i.e., a 2 cm shift in PCD is amplified five times in the dimensions of the detected obstacles, is well observed for all the models and almost all the perturbations.** TED is robust against three perturbation types and Voxel RCNN is immune to two perturbation types. While these models show more robustness, the fact that they only detect cars contributes since cars are larger, thus car detection is more resistant to minor perturbations.

The most ineffective perturbation of *SORBET* is false positive (FP). This is unsurprising since FP removes only one point from 10,000 points. Considering the number of points representing an obstacle, FP at most removes one point. Still, two models (Point RCNN and Apollo) show non-trivial reduced performance, i.e., these two are quite impacted by an

extremely slight change (at most two points are removed in the PCD). Upon further investigation, models such as Apollo’s are impacted by such minimal change because they rely heavily on the aggregated confidence score (all points in a detected region) for filtering. FP impacts the model performance as the aggregated confidence would fall below a defined threshold with points removed. Hence, we observe that (1) the deviation is significantly smaller than other types of perturbations; (2) these two systems are more sensitive compared to others. This suggests that this type of perturbation while having the potential to cause deviations, is more likely to impact older and more sensitive 3D obstacle detection systems.

Our experiments show that range inaccuracy (global) can cause significant deviations (of more than 0.1 meters) in 3D obstacle detection for up to 20% of the obstacles. Also, we observe a non-trivial number of obstacles with very significant deviations of more than 0.5 IoU changes which is visualized in Figure 4. This shows that considerable deviation in the IoU

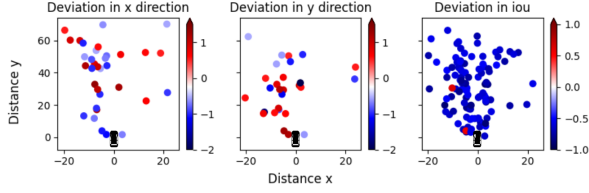


Fig. 4: Deviations in x, y, and IoU metrics for detected obstacles by PointPillar when there are range inaccuracies. Only coordinates deviations greater than ± 0.5 m and IoU deviations greater than ± 0.5 are shown. The black car at (0, 0) shows the location of the ego car.

is caused by hardly visible perturbations.

Perturbations of type **range inaccuracy (local)** result in fewer obstacles having large deviations and smaller decreases in detected obstacles. While the range of deviation of each dimension remains similar, obstacle-specific perturbations cause fewer undetected obstacles compared to the non-target version. Perturbations generated by uniform randomization even result in zero deviations. We suspect that this is caused by multiple factors. First, we observe that for detected obstacles in the baselines, the average IoU (excluding those less than 0.25) is between 0.7 and 0.8, which means the bounding box generated by the model has a large offset from ground truth under “noise-free” conditions. This reduces the efficiency of obstacle-specific perturbations. This brings us to the second point that detections are likely impacted by both the points inside and outside of the projected bounding box, thus only changing the point inside the ground truth bounding box may not cause as much impact as expected. While the deviation caused by targeted perturbations is not as pronounced as we expected, we still observe non-trivial deviations.

Then, for distance-amplified range inaccuracy (directional), we observe significant deviations with more obstacles that have large deviations when compared to range inaccuracy (local), even on par with range inaccuracy (global) in some models. The output confirms our intuition that perturbations applied in the same direction magnify the impact of the perturbation. The results show that even very small perturbations added to a few points in the PCD (less than 1.5%) can cause non-trivial deviations in obstacle detection.

In our experiments, reflectivity noises significantly impact IoU decreases and undetected obstacles compared to previous perturbations when we decrease the number of points belonging to the ground truth obstacles by 60%. As shown in Figure 5a, we see a large decrease in the number of obstacles detected (between 10% and 24%) and a significant increase in the number of detected obstacles with large deviations. The reverse (i.e., reducing reflectivity) does not have as much impact. When we increase the number of points in the bounding boxes of ground-truth obstacles by 67%, we do not observe a significant deviation as when we decrease it. However, we observe that while we cause a significant amount of change to the number of points in bounding boxes (over 1.5% of each frame on average) the deviation is very similar to range inaccuracy (global) and even causes fewer differences

in obstacles detected compared to the baseline.

Lastly for distance-amplified range inaccuracy, while the number of obstacles detected is slightly less than range inaccuracy (global), we observe up to 290% increase in the number of obstacles that have large deviations.

Overall, we observe that while the degree of deviation resulting from the perturbations differs between different models, the trend is the same.

RQ1 Finding: Our experiments show that while models are robust for average cases, small, random perturbations can still cause significant deviations to the detection results, e.g., up to 17.5% of the obstacles have significantly different results, either the obstacles not detected at all, or a large deviation observed for dimensions and size.

RQ2: What are the cascading impacts on ADSs caused by the perturbations of the LiDAR’s PCD input?

Motivation. In the previous RQ, we learned that even minimal perturbations can cause considerable deviations in the obstacle detection results. Thus, we are interested to learn how this will affect the following modules, i.e., trajectory prediction. In particular, we are intrigued to learn how these detection deviations from obstacle detection can further impact the trajectory prediction process and cause more deviations. As the trajectory depends on the position of the obstacle in the previous frames, these deviations have the potential to change the predicted trajectory and possibly the planned ego trajectory. **Note that the fewer-detected obstacles (the rows of ‘DIFF’ in Table IV) would cause adverse impacts on the safety ADS. Hence, our focus in this RQ is on the large deviations of the dimensions (x and y).** In this RQ, we aim to quantify the degree of change caused by this deviation and evaluate whether they are significant enough to cause adverse effects to be functions of the ego car.

Method. Our goal is to perform a comprehensive study to understand how the fluctuated PCDs (from LiDAR) would impact a subsequent decision-making module (i.e., trajectory prediction) in a cascading fashion, i.e., such fluctuations cause deviated detection results, which further impact trajectory prediction. As trajectory prediction works on a set of consecutive frames (i.e., 10 - 15 frames/s) we opt for a trajectory dataset, i.e., nuScenes [8] for this experiment as the KITTI dataset contains non-consecutive frames.

The first step involves extracting the deviations obtained from RQ1 on the range of expected x and y deviations from providing the perturbed PCD to Apollo. We filter out the data from obstacles further than ten meters from the ego as we want to focus on close obstacles that are more impactful. From this data, we calculate the deviation in x and y at different percentiles including outliers for Apollo’s obstacle detection. Assuming the normal distribution of the deviations, we use the points that represent the Q1 (25%), median (50%), and Q3 (75%) in both the x and y directions as our perturbations to the ground truth. In addition to that, we partition the outliers into two parts, those that are greater than the upper fence (UF) ($Q3 + 1.5 * IQR$) (95%) and those that are less than the lower

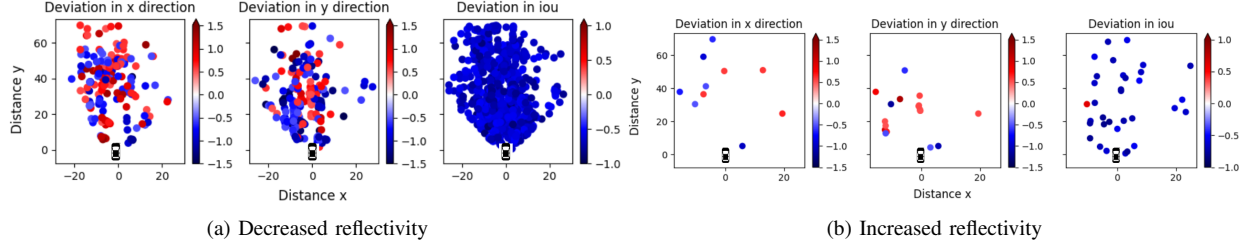


Fig. 5: Deviations in x, y, and IoU metrics for detected obstacles by PointPillar when the perturbations are generated based on reflectivity and apply to points that belonged to obstacles. Only coordinates deviations greater than ± 0.5 and IoU deviations greater than ± 0.5 are shown.

fence (LF) (Q1 - 1.5 * IQR) (5%), outliers (1%) and select the minimum, maximum, and the median from each group.

The second step is to generate input data with the perturbations as described in the first step. For Trajectron++, the input is generated from the nuScenes data set. To obtain the baseline trajectory in this case, we run the Trajectron++ base model on all obstacles from 150 scenes in the test set of nuScenes and record the predicted trajectory. For Apollo, the input is the simulation ground truth. For the simulation, we set up a scenario in the simulation where the obstacle and car run in the same direction for ten seconds in parallel lanes. We record this trajectory as the baseline trajectory.

Apollo is used in combination with a simulator, to address the limitation of an unstable environment brought by the simulator, we opted to repeat the simulation twenty times for each perturbation type. We run the simulation process without any perturbation twenty times to establish a baseline and for each of the perturbations, we re-run the simulation twenty times. Then to compute the differences, we identify the most common frame that the obstacle is received, the location of the obstacle at this point, and the frame at which the first prediction is made. Anything not fitting this common profile is filtered out. Note that the location of the original obstacle in LGSVL remains the same, we are only adding perturbations based on calculated deviations measured previously to the input of the prediction module.

We try the following patterns of integrating perturbed detection results on a series of consecutive frames and computing the deviation between the new trajectory and the old trajectory. We believe the patterns are realistic given the naturalness and commonality of *SORBET*'s perturbations.

- 1) Interval: Perturbations applied at an interval (once every three frames).
- 2) All: Perturbation applied every frame.
- 3) Remove Once: Replace the position of the obstacle with the values of the previous frame.

In the final step, we select the cases with significant deviations and lane-changing deviations as obtained from the simulation and re-run these simulations while monitoring the output from the planning module in Apollo. We would monitor how much the planned trajectory changes under baseline conditions as the control. Then, we would measure the resulting deviations that are caused by the changed obstacle trajectory. This would reveal how much of the ego's planned trajectory

is affected by the original perturbations, and whether it results in adverse effects such as unnecessary stops, or other changes in the planning decisions.

Results. We use the following error metrics commonly used in prior works [32], [49]. A predicted trajectory contains a series of predicted positions for one detected obstacle.

- 1) *Average displacement error (ADE)*: Root mean square error (RMSE) between the original and the deviated predicted trajectory. We compute this for the x and y directions separately
- 2) *Final displacement error (FDE)*: RMSE between the final predicted position between the baseline and the perturbed trajectory. We compute this separately for the x and y directions

For this analysis, we will consider an average car to have dimensions similar to the one in KITTI [7] which has a width of 1.6 meters. Considering the average lane to be 3.6 meters [52]. Assuming the car to be keeping the center of its lane, the distance from the side of the car to the lane line is 1 meter.

TABLE V: Top one percent deviations for Trajectron++ (base) on nuScene. Units are in meters.

	Perturbations		Trajectron++ (1s)			
			ADE/FDE Interval		ADE/FDE All	
Meaning	+ x	+ y	x	y	x	y
baseline	+ 0	+ 0	0.0/0.0	0.0/0.0	0.0/0.0	0.0/0.0
x Q1	- 0.04	+ 0.01	0.09/0.12	0.11/0.14	0.04/0.04	0.01/0.01
x Q3	+ 0.0	- 0.02	0.04/0.06	0.05/0.07	0.0/0.0	0.02/0.02
y Q1	- 0.05	- 0.03	0.13/0.16	0.12/0.17	0.05/0.05	0.03/0.03
y Q3	- 0.06	+ 0.02	0.11/0.14	0.14/0.19	0.06/0.06	0.02/0.02
x UF	+ 0.06	- 0.03	0.12/0.16	0.11/0.16	0.06/0.06	0.03/0.03
x LF	- 0.10	- 0.04	0.15/0.18	0.13/0.21	0.10/0.10	0.04/0.04
y UF	- 0.05	+ 0.08	0.10/0.14	0.17/0.21	0.05/0.05	0.08/0.08
y LF	- 0.03	- 0.09	0.10/0.14	0.17/0.21	0.03/0.03	0.09/0.09
x outlier	- 0.34	- 0.58	0.51/0.67	0.68/0.77	0.34/0.34	0.58/0.58
y outlier	- 0.13	- 0.14	0.19/0.23	0.22/0.25	0.13/0.13	0.14/0.14
x min	- 5.90	- 3.16	7.04/8.63	3.70/4.52	5.91/5.93	3.18/3.20
x/y max	+ 0.53	+ 0.41	0.66/0.80	0.52/0.59	0.53/0.53	0.41/0.41
y min	- 5.37	- 3.24	6.46/7.97	3.72/4.46	5.38/5.39	3.26/3.27

First, we will discuss the average case for observed deviations found in Trajectron++ when we introduce the perturbations. When all of the ground truth positions are perturbed, the deviation measured by the ADE and the FDE is very close to that of the introduced perturbation, with the largest observed deviation being less than 0.1 meters. When perturbations are applied at an interval (one every three frames), we observe

TABLE VI: Perturbations to the ground truth obstacle and resulting deviations for Trajectron++ (base) on nuScenes. The greater value between the ADE and FDE is highlighted in **bold**. Units are in meters.

Trajectron++ (1s)		ADE/FDE Remove Once	
Average case		Top 1%	
x	y	x	y
0.00/0.00	0.00/0.00	0.00/0.00	0.00/0.00
1.82/1.24	0.97/1.11	7.27/9.77	6.41/8.41

that the resulting deviation is still very close to the introduced perturbation, with the largest ADE/FDE observed being less than 0.16 meters. For the relationship between FDE and ADE, they are identical except for when the perturbation is applied at an interval. Then, the FDE can be up to two centimeters larger than the ADE.

The top 1% of the deviations (by value) show non-trivial deviations (Table V). Here, we observe significant deviations when the perturbation is applied at an interval. The resulting ADE can be up to two times the original perturbation, and the FDE can even be up to 2.5 times. For example, in the extreme case of Figure 6, we observe that the obstacle on the lane has its trajectory miscalculated to be on the sidewalk, which will result in incorrect planning. However, we observe that

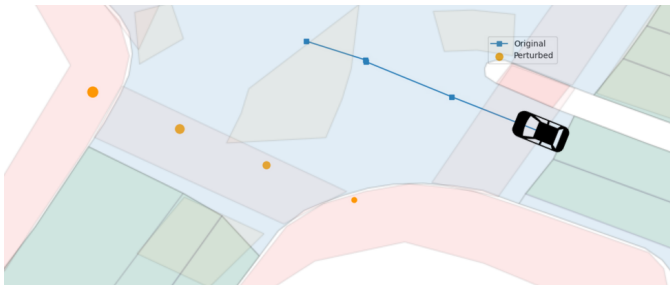


Fig. 6: An example of an extreme outlier (minimum x deviation observed from Apollo in RQ1) observed from Trajectron++ trajectory prediction where the original trajectory (blue) is miscalculated to be on the sidewalk (orange).

for most cases, the resulting deviation is less than 0.3 meters, meaning the car is not predicted to change lanes. Even for large deviations such as the x outlier case, the obstacle is not predicted to change lanes. Obviously, this assessment is under the assumption that the obstacle is currently in the middle of the lane. However, this deviation can change the ego's planning process is close to the lane line.

For perturbation where we remove only one frame from the original location used for trajectory prediction (Table VI, we observe significant ADE and FDE for only a single frame change. Both the ADE and the FDE show more than one-meter changes for each point in the predicted trajectory, which can cause a significant impact on other obstacles in nearby lanes. Moreover, as observed in Table V, the top 1% can cause several meters of deviation. This has a significant impact on the behaviors of other obstacles on the road, especially ADS which has planning modules.

In Apollo, we record the cases fitting the profile to improve reproducibility. For our analysis, we take the average of these

TABLE VII: Deviations of Apollo in simulation. Units are in meters.

Meaning	Apollo (0.8s)			
	ADE/FDE Interval		ADE/FDE All	
	x	y	x	y
baseline	0.00/0.00	0.000/0.000	0.00/0.00	0.00/0.00
x Q1	0.0/0.0	1.08/1.82	0.21/0.29	4.38/8.12
x Q3	0.20/0.25	3.37/6.36	0.16/0.17	4.16/7.19
y Q1	0.15/0.22	4.14/7.45	0.21/0.34	5.41/10.42
y Q3	0.22/0.27	4.04/7.65	0.79/1.14	11.32/21.79
x UF	0.02/0.0	0.79/1.18	0.31/0.40	3.22/6.36
x LF	0.34/0.51	6.31/11.77	0.50/0.72	9.79/18.0
y UF	0.18/0.27	4.47/8.27	0.74/1.09	11.03/21.28
y LF	0.52/0.77	10.11/19.10	0.28/0.40	3.86/7.53
x outlier	0.0/0.0	1.08/1.82	0.31/0.0	1.24/2.0
y outlier	0.03/0.01	3.60/5.92	0.22/0.24	2.8/5.28
x min	2.69/3.50	9.23/15.33	0.01/0.0	0.18/0.36
y min	2.73/3.47	8.57/14.20	0.31/0.51	6.74/12.94
x/y max	0.04/0.02	5.64/9.31	0.21/0.23	0.75/1.62

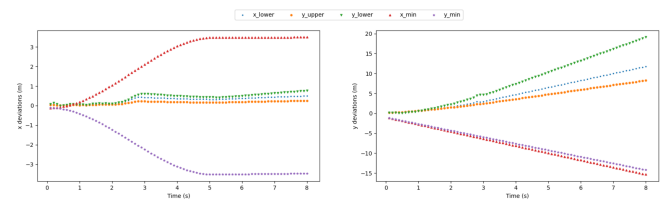


Fig. 7: Figure showing the deviations in the prediction trajectory in Apollo w.r.t the baseline when the perturbations are applied at an interval.

remaining cases. Figure 7 shows the resulting deviation in the trajectory when the perturbations are applied at an interval. As also confirmed by Table VII, perturbations in the x direction resulted in smaller deviations than in the y direction. We can observe that for x, if not consider the min/max values perturbation cases, most deviations cause very small changes in trajectory prediction (less than 0.3 m) similar to Trajectron++. However, the large deviations in this case are significant and are highly likely to cause a change to path planning with the possibility of making the ego stop unnecessarily.

For the perturbations rounds, we categorize them based on the frames where the obstacles are detected, the frame where the trajectories are computed, and the position of the obstacle at the point where the trajectory is predicted. The cases in Table VII are predicted at the 0.8s point, where the trajectory prediction module in Apollo makes the first prediction after seven to eight frames of location data from obstacle detection. In Apollo, we observe larger deviations than in Trajectron++.

When perturbations are applied to all frames instead of only at an interval, we observe a significant increase in deviations. This is surprising since it is the opposite of what we found in Trajectron++. From this, we can see that perturbations (less than two centimeters) can cause deviations large enough to change the trajectory of the obstacles, even in state-of-the-art ADS such as Apollo. However, the changed trajectory deviates very little from the baseline for most observed cases. Even when there are significant deviations that change the prediction and planning, the adverse effects are not guaranteed to

manifest since both prediction and planning decisions change frequently. This still raises concerns about the robustness of obstacles perception meant to be used for ADS and ADS themselves to provide safeguard measures and improve the safety of their products since wrong decisions/actions even if happen momentarily, can raise safety issues.

RQ2 Finding: Our experiment shows that while trajectory predictors are robust to perturbations on most moderate cases (50%), very small built-in perturbations can still cause significant deviations to the trajectory prediction results. The impact on the y dimension (the distance to the ego car in its moving direction) is more significant than the x dimension.

RQ3: Can the perturbations improve the robustness of ADSs?

Motivation. Our work focuses on testing and is not adversarial attacks. Nevertheless, it is valuable to understand how to address the issues found. Previous works improve 3D obstacle detection via retraining with the perturbed data or pre-processing to smooth the inaccurate data. As a preliminary experiment, we opt to retrain the OpenPCDet models with a new training data set.

Method. As a preliminary study, we use a naive method to retrain the models. We retrain the models with a new training dataset, which is the same size as the original and is composed of 33% original and 67% perturbed PCD from Uniform Range Inaccuracy (Global).

Results. The results (Table VIII) show even a naive method

TABLE VIII: Retrain

Model	DIFF	Detections	mAP (Cars)
Point Pillar	6.7	0.9	0.5
Point RCNN	0.8	1.2	-0.5
Voxel RCNN	10.6	0.3	0.3
TED	0.0	0.0	0.0

can improve performance. For all models, we observe better robustness against the minor perturbations, i.e., reducing DIFF (Table IV) by 0.8%-10.6%. The retrained model shows slightly better performance in both original and perturbed test datasets for Point Pillar and Voxel RCNN, i.e., the retrained models detect 0.3%-0.9% more ground-truth obstacles. For the mAP, we observe no clear trend. As TED is resistant to this perturbation (Table IV), it is unaffected. We will continue the experiment on retraining in the next version of the study.

VI. THREATS TO VALIDITY

Internal Threats. Some models in the study are unstable which can cause errors. Hence, we run the models five times for each input and take the average of all measurements. In our results, while these models always have a small deviation, they conform to the trend of increase/decrease in deviation similar to the more stable models.

External Threats. We focus on the Velodyne HDL-64E which records the KITTI data set and is used by Apollo. However, the documents that describe this sensor differ in its accuracy. While specification [6] show the accuracy within 5 cm, the

KITTI paper [7] describes the points' accuracy as within 2 cm. We use the lower number [7] because if the lower number can cause noticeable deviations, the larger would exacerbate the issue, contributing more to our conclusion.

Construction Threats. Our obstacle-specific perturbations are computed based on the ground truth dimensions to the best of our ability. While this is meant to be generalizable to multiple models, the median IoU between the detections and the ground truth is mostly between 70%-80% which means the perturbations cause less impact than expected. Yet, we have already observed non-trivial deviations.

When adding perturbations to the trajectory prediction input for Apollo, we re-direct the data (Section III-D). This risks delays changing the number of predictions. For our experiment, we compared the trajectory prediction before and after our code was added and found no impact on the number of prediction and their timeliness. However, this can cause delays or frame drops.

VII. CONCLUSION

Our contributions highlight the necessity of evaluating the robustness of obstacle detection models against built-in inaccuracies of LiDAR sensors. We also demonstrate that such built-in inaccuracies have cascading negative impacts on the subsequent trajectory prediction module. Our results show that models have different robustness capabilities against sensor inaccuracies and this should be considered when selecting models. The minor-perturbed data set can improve the performance of obstacle detection modules. Practitioners should incorporate robustness testing and examine the LiDAR inaccuracies carefully when developing ADS. The implementation of SORBET is available at [6] for reference.

REFERENCES

- [1] S. Tang, Z. Zhang, Y. Zhang, J. Zhou, Y. ling Guo, S. Liu, S. Guo, Y. Li, L. Ma, Y. Xue, and Y. Liu, "A survey on automated driving system testing: Landscapes and trends," *ACM Transactions on Software Engineering and Methodology*, vol. 32, pp. 1 – 62, 2022.
- [2] T. Mawakana and D. Dolgov. (2023) Doubling down on waymo one. [Online]. Available: <https://waymo.com/blog/2023/07/doubling-down-on-waymo-one.html>
- [3] E. Ludlow. (2023) Paid driverless taxis are slowly becoming a reality. [Online]. Available: <https://www.bloomberg.com/news/newsletters/2023-08-16/paid-driverless-taxis-are-slowly-becoming-a-reality>
- [4] KPMG. (2023) The rise of the driverless vehicle. [Online]. Available: <https://kpmg.com/ca/en/home/market-insights/predictions/economy-and-markets/the-rise-of-the-driverless-vehicle.html>
- [5] J. Cui, L. S. Liew, G. Sabaliauskaite, and F. Zhou, "A review on safety failures, security attacks, and available countermeasures for autonomous vehicles," *Ad Hoc Networks*, vol. 90, 2019.
- [6] L. Manuals. (2023) Specification sheets for lidar sensors. [Online]. Available: https://github.com/anonfolders/lidar_robustness
- [7] A. Geiger, P. Lenz, and R. Urtasun, "Are we ready for autonomous driving? the kitti vision benchmark suite," in *Conference on Computer Vision and Pattern Recognition (CVPR)*, 2012.
- [8] H. Caesar, V. Bankiti, A. H. Lang, S. Vora, V. E. Liong, Q. Xu, A. Krishnan, Y. Pan, G. Baldan, and O. Beijbom, "nuscenes: A multimodal dataset for autonomous driving," in *CVPR*, 2020.
- [9] X. Xu, J. Zhang, Y. Li, Y. Wang, Y. Yang, and H. T. Shen, "Adversarial attack against urban scene segmentation for autonomous vehicles," *IEEE Transactions on Industrial Informatics*, vol. 17, pp. 4117–4126, 2021.
- [10] Y. Cao, C. Xiao, B. Cyr, Y. Zhou, W. Park, S. Rampazzi, Q. A. Chen, K. Fu, and Z. M. Mao, "Adversarial sensor attack on LiDAR-based perception in autonomous driving," in *Proceedings of the 2019 ACM SIGSAC Conference on Computer and Communications Security*. ACM, nov 2019.

- [11] Y. Cao, N. Wang, C. Xiao, D. Yang, J. Fang, R. Yang, Q. A. Chen, M. Liu, and B. Li, "Invisible for both camera and lidar: Security of multi-sensor fusion based perception in autonomous driving under physical-world attacks," in *2021 IEEE Symposium on Security and Privacy (SP)*, May 2021, pp. 176–194.
- [12] J. Sun, Q. Zhang, B. Kailkhura, Z. Yu, C. Xiao, and Z. M. Mao, "Benchmarking robustness of 3d point cloud recognition against common corruptions," *ArXiv*, vol. abs/2201.12296, 2022.
- [13] Z. Q. Zhou and L. Sun, "Metamorphic testing of driverless cars," *Commun. ACM*, vol. 62, no. 3, p. 61–67, feb 2019.
- [14] K. Yu, T. Tao, H. Xie, Z. Lin, Z. Wu, Z. Xia, T. Liang, H. Sun, J. Deng, D. Hao, Y. Wang, X. Liang, and B. Wang, "Benchmarking the robustness of lidar-camera fusion for 3d object detection," 2022.
- [15] X. Gao, Z. Wang, Y. Feng, L. Ma, Z. Chen, and B. Xu, "Benchmarking robustness of ai-enabled multi-sensor fusion systems: Challenges and opportunities," *ArXiv*, vol. abs/2306.03454, 2023.
- [16] F. Albreiki, S. Abughazal, J. Lahoud, R. M. Anwer, H. Cholakkal, and F. S. Khan, "On the robustness of 3d object detectors," *Proceedings of the 4th ACM International Conference on Multimedia in Asia*, 2022.
- [17] S. Zheng, W. Liu, S. Shen, Y. Zang, C. Wen, M. Cheng, and C. Wang, "Adaptive local adversarial attacks on 3d point clouds," *Pattern Recognition*, vol. 144, p. 109825, 2023.
- [18] H. Shin, D. Kim, Y. Kwon, and Y. Kim, "Illusion and dazzle: Adversarial optical channel exploits against lidars for automotive applications," in *Cryptographic Hardware and Embedded Systems – CHES 2017*, W. Fischer and N. Homma, Eds. Cham: Springer International Publishing, 2017, pp. 445–467.
- [19] J. Sun, Y. Cao, Q. A. Chen, and Z. M. Mao, "Towards robust lidar-based perception in autonomous driving: General black-box adversarial sensor attack and countermeasures," in *Proceedings of the 29th USENIX Conference on Security Symposium*, ser. SEC'20. USA: USENIX Association, 2020.
- [20] X. Wang, M. Cai, F. Sohel, N. Sang, and Z. Chang, "Adversarial point cloud perturbations against 3d object detection in autonomous driving systems," *Neurocomputing*, vol. 466, pp. 27–36, 2021.
- [21] Y. Zhu, C. Miao, T. Zheng, F. Hajiaghajani, L. Su, and C. Qiao, "Can we use arbitrary objects to attack lidar perception in autonomous driving?" in *Proceedings of the 2021 ACM SIGSAC Conference on Computer and Communications Security*, ser. CCS '21. New York, NY, USA: Association for Computing Machinery, 2021, p. 1945–1960.
- [22] Y. Zhu, C. Miao, F. Hajiaghajani, M. Huai, L. Su, and C. Qiao, "Adversarial attacks against lidar semantic segmentation in autonomous driving," *Proceedings of the 19th ACM Conference on Embedded Networked Sensor Systems*, 2021.
- [23] K. Yang, T. Tsai, H. Yu, M. Panoff, T.-Y. Ho, and Y. Jin, "Robust roadside physical adversarial attack against deep learning in lidar perception modules," *Proceedings of the 2021 ACM Asia Conference on Computer and Communications Security*, 2021.
- [24] Z. Hau, K. T. Co, S. Demetriou, and E. C. Lupu, "Object removal attacks on lidar-based 3d object detectors," *ArXiv*, vol. abs/2102.03722, 2021.
- [25] Z. Xiong, H. Xu, W. Li, and Z. Cai, "Multi-source adversarial sample attack on autonomous vehicles," *IEEE Transactions on Vehicular Technology*, vol. 70, no. 3, pp. 2822–2835, 2021.
- [26] M. Abdelfattah, K. Yuan, Z. J. Wang, and R. Ward, "Towards universal physical attacks on cascaded camera-lidar 3d object detection models," in *2021 IEEE International Conference on Image Processing (ICIP)*, 2021, pp. 3592–3596.
- [27] J. Tu, H. Li, X. Yan, M. Ren, Y. Chen, M. Liang, E. Bitar, E. Yumer, and R. Urtasun, "Exploring adversarial robustness of multi-sensor perception systems in self driving," in *Proceedings of the 5th Conference on Robot Learning*, ser. Proceedings of Machine Learning Research, A. Faust, D. Hsu, and G. Neumann, Eds., vol. 164. PMLR, 08–11 Nov 2022, pp. 1013–1024.
- [28] J. Tu, M. Ren, S. Manivasagam, M. Liang, B. Yang, R. Du, F. Cheng, and R. Urtasun, "Physically realizable adversarial examples for lidar object detection," in *Proceedings of the IEEE/CVF Conference on Computer Vision and Pattern Recognition (CVPR)*, June 2020.
- [29] B. Liu, Y. Guo, J. Jiang, J. Tang, and W. Deng, "Multi-view correlation based black-box adversarial attack for 3d object detection," in *Proceedings of the 27th ACM SIGKDD Conference on Knowledge Discovery & Data Mining*, ser. KDD '21. New York, NY, USA: Association for Computing Machinery, 2021, p. 1036–1044.
- [30] Baidu. (2023) Baidu apollo. [Online]. Available: <https://github.com/ApolloAuto/apollo/>
- [31] Z. Peng, J. Yang, T.-H. P. Chen, and L. Ma, "A first look at the integration of machine learning models in complex autonomous driving systems: A case study on apollo," in *Proceedings of the 28th ACM Joint Meeting on European Software Engineering Conference and Symposium on the Foundations of Software Engineering*, ser. ESEC/FSE 2020. New York, NY, USA: Association for Computing Machinery, 2020, p. 1240–1250.
- [32] Q. Zhang, S. Hu, J. Sun, Q. A. Chen, and Z. M. Mao, "On adversarial robustness of trajectory prediction for autonomous vehicles," in *Proceedings of the IEEE/CVF Conference on Computer Vision and Pattern Recognition (CVPR)*, June 2022, pp. 15 159–15 168.
- [33] Y. Jia, Y. Lu, J. Shen, Q. A. Chen, Z. Zhong, and T. Wei, "Fooling detection alone is not enough: First adversarial attack against multiple object tracking," 2019.
- [34] Y. Li, C. Wen, F. Juefei-Xu, and C. Feng, "Fooling lidar perception via adversarial trajectory perturbation," 2021.
- [35] J. Wang, A. Pun, J. Tu, S. Manivasagam, A. Sadat, S. Casas, M. Ren, and R. Urtasun, "Advsim: Generating safety-critical scenarios for self-driving vehicles," in *2021 IEEE/CVF Conference on Computer Vision and Pattern Recognition (CVPR)*, 2021, pp. 9904–9913.
- [36] S. Saadatnejad, M. Bahari, P. Khorsandi, M. Saneian, S.-M. Moosavi-Dezfooli, and A. Alahi, "Are socially-aware trajectory prediction models really socially-aware?" *Transportation Research Part C: Emerging Technologies*, vol. 141, p. 103705, 2022.
- [37] J. C. Han and Z. Q. Zhou, "Metamorphic fuzz testing of autonomous vehicles," in *Proceedings of the IEEE/ACM 42nd International Conference on Software Engineering Workshops*, ser. ICSEW'20. New York, NY, USA: Association for Computing Machinery, 2020, p. 380–385.
- [38] R. Jiao, X. Liu, T. Sato, Q. A. Chen, and Q. Zhu, "Semi-supervised semantics-guided adversarial training for trajectory prediction," *ArXiv*, vol. abs/2205.14230, 2022.
- [39] A. Guo, Y. Feng, and Z. Chen, "Lirtest: Augmenting lidar point clouds for automated testing of autonomous driving systems," in *Proceedings of the 31st ACM SIGSOFT International Symposium on Software Testing and Analysis*, ser. ISSTA 2022. New York, NY, USA: Association for Computing Machinery, 2022, p. 480–492.
- [40] A. Dosovitskiy, G. Ros, F. Codevilla, A. M. López, and V. Koltun, "Carla: An open urban driving simulator," in *Conference on Robot Learning*, 2017.
- [41] S. Shah, D. Dey, C. Lovett, and A. Kapoor, "Airsim: High-fidelity visual and physical simulation for autonomous vehicles," in *Field and Service Robotics*, M. Hutter and R. Siegwart, Eds. Cham: Springer International Publishing, 2018, pp. 621–635.
- [42] W. Jansen, N. Huebel, and J. Steckel, "Physical lidar simulation in real-time engine," in *2022 IEEE Sensors*, 2022, pp. 1–4.
- [43] G. J. Sequeira, B. Harlapur, D. O. Ortegón, R. Lugner, T. Brandmeier, and V. Soloiu, "Investigation of influence from variation in color on lidar sensor for perception of environment in autonomous vehicles," in *2021 International Symposium ELMAR*, 2021, pp. 71–76.
- [44] LGSVL. (2021) Lgsvl simulator. [Online]. Available: <https://github.com/lgsvl/simulator/>
- [45] A. H. Lang, S. Vora, H. Caesar, L. Zhou, J. Yang, and O. Beijbom, "Pointpillars: Fast encoders for object detection from point clouds," 2019.
- [46] S. Shi, X. Wang, and H. Li, "Pointtrnn: 3d object proposal generation and detection from point cloud," *2019 IEEE/CVF Conference on Computer Vision and Pattern Recognition (CVPR)*, pp. 770–779, 2018.
- [47] J. Deng, S. Shi, P. Li, W. Zhou, Y. Zhang, and H. Li, "Voxel r-cnn: Towards high performance voxel-based 3d object detection," 2021.
- [48] H. Wu, C. Wen, W. Li, R. Yang, and C. Wang, "Transformation-equivariant 3d object detection for autonomous driving," in *AAAI*, 2023.
- [49] T. Salzmänn, B. Ivanovic, P. Chakravarty, and M. Pavone, "Trajectron++: Dynamically-feasible trajectory forecasting with heterogeneous data," 2021.
- [50] OpenPCDet, "Openpcdet: An open-source toolbox for 3d object detection from point clouds," <https://github.com/open-mmlab/OpenPCDet>, 2020.
- [51] G. Li, Y. Li, S. Jha, T. Tsai, M. Sullivan, S. K. S. Hari, Z. Kalbarczyk, and R. Iyer, "Av-fuzzer: Finding safety violations in autonomous driving systems," in *2020 IEEE 31st International Symposium on Software Reliability Engineering (ISSRE)*, 2020, pp. 25–36.
- [52] Staff, *A Policy on Geometric Design of Highways and Streets (4th ed.)*. Washington: American Association of State Highway and Transportation Officials, 2001.